

# Design and performance of dual-band MWIR/LWIR focal plane arrays based on a type-II superlattice nBn structure

Hyun-Jin Lee<sup>1\*</sup>, Jun Ho Eom<sup>1</sup>, Hyun Chul Jung<sup>1</sup>, Ko-Ku Kang<sup>1</sup>, Seong Min Ryu<sup>1</sup>, Ahreum Jang<sup>1</sup>, Jong Gi Kim<sup>1</sup>, Young Ho Kim<sup>1</sup>, Han Jung<sup>1</sup>, Sun Ho Kim<sup>2</sup>, Jong Hwa Choi<sup>2</sup>

<sup>1</sup>i3system, Inc., 26-32, Gajeongbuk-ro, Yuseong-gu, Daejeon, 34113, Republic of Korea

<sup>2</sup>Agency of Defense Development, 34186 P.O.Box 35, Yuseong-gu, Daejeon, Republic of Korea

## Article info

### Article history:

Received 15 Oct. 2022

Received in revised form 10 Dec. 2022

Accepted 19 Dec. 2022

Available on-line 24 Feb. 2023

### Keywords:

InAs/GaSb type-II superlattice; dual-band detector; dark current; spectral quantum efficiency; noise equivalent temperature difference.

## Abstract

Dual-band infrared detector, which acquires more image information than single-band detectors, has excellent detection, recognition, and identification capabilities. The dual-band detector can have two bumps to connect with each absorber layer, but it is difficult to implement small pitch focal plane arrays and its fabrication process is complicated. Therefore, the most effective way for a dual-band detector is to acquire each band by bias-selectable with one bump. To aim this, a dual-band MWIR/LWIR detector based on an InAs/GaSb type-II superlattice nBn structure was designed and its performance was evaluated in this work. Since two absorber layers were separated by the barrier layer, each band can be detected by bias-selectable with one bump. The fabricated dual-band device exhibited the dark current and spectral response characteristics of MWIR and LWIR bands under negative and positive bias, respectively. Spectral crosstalk that is a major issue in dual-band detectors was also improved. Finally, a 20  $\mu\text{m}$  pitch  $640 \times 512$  dual-band detector was fabricated, and both MWIR and LWIR images exhibited an average noise equivalent temperature difference of 30 mK or less at 80 K.

## 1. Introduction

MWIR and LWIR detectors, which are widely used in guided weapon and surveillance reconnaissance systems, are advantageous for detecting hot and cool objects, respectively [1, 2]. Dual-band infrared detector that can acquire MWIR and LWIR image information with a single detector has excellent detection, recognition, and identification (DRI) capabilities. The simplest method for dual-band detector is to package each band focal plane arrays (FPAs) into a single dewar, but it is very bulky, and its cooling power consumption is high. Therefore, various research groups have studied dual-band or multi-band detectors on-chip since 1998 [3–6]. Dual-band on-chip detector is implemented by sequentially growing each absorber layer in an epi. wafer, and then two electrodes (bumps) are formed to connect to each absorber [6–8]. This way can detect two bands at the same time, which can

increase the frame rate of the detector. However, it can be difficult to fabricate small pitch and large format FPAs. Another way is to use a unipolar barrier structure [9–11]. The dual-band detector with a unipolar barrier structure acquires each band by sequentially selecting the applied bias with only one electrode (bump). Therefore, it is possible to fabricate a small pitch and large format dual-band detector.

In this work, a dual-band MWIR/LWIR detector with an InAs/GaSb type-II superlattice (T2SL) nBn structure was designed and fabricated. Its properties in terms of dark current, spectral quantum efficiency (QE), and spectral crosstalk were evaluated. In addition, a 20  $\mu\text{m}$  pitch  $640 \times 512$  read-out integrated circuit (ROIC) capable of bias-switching with one bump was designed and manufactured to evaluate the optical performance of the dual-MWIR/LWIR FPA. The fabricated FPAs exhibited an average noise equivalent temperature difference (NETD) of less than 30 mK at 80 K.

\*Corresponding author at: [leehj@i3system.com](mailto:leehj@i3system.com)

## 2. Epi. structure for dual-band MWIR/LWIR device

The epi. structure for the dual-band MWIR/LWIR was designed using the InAs/GaSb T2SL. MWIR absorber was designed and added to the InAs/GaSb LWIR nBn structure reported in previous studies [12, 13]. As shown in Fig. 1, LWIR absorber, barrier and MWIR absorber layers were designed as InAs/GaSb 14/7 monolayers (MLs), 4/9 MLs and 10/10 MLs, respectively. Each bandgap energy calculated using the eight-band  $\mathbf{k}\cdot\mathbf{p}$  numerical method is  $\sim 0.134$  eV for LWIR absorber,  $\sim 0.544$  eV for barrier, and  $\sim 0.249$  eV for MWIR absorber.

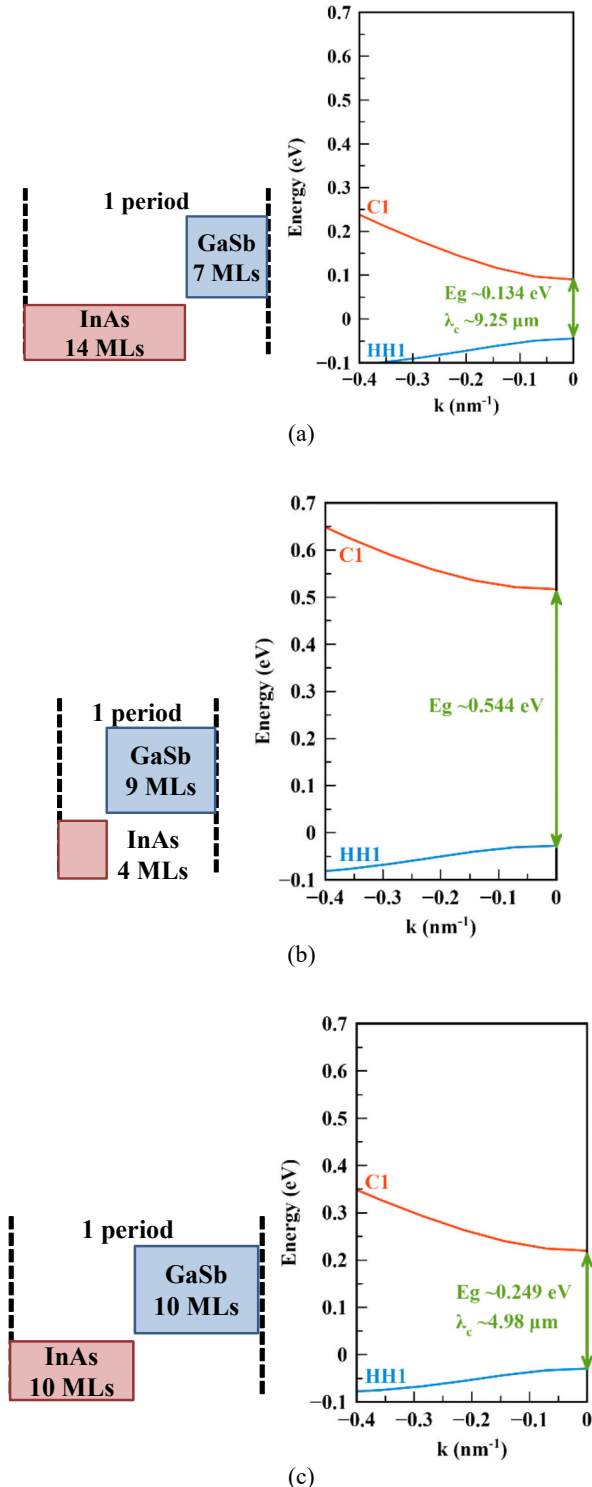


Fig. 1. Design details of epi. structure for dual-band nBn: LWIR absorber (a), barrier (b), and MWIR absorber (c).

The epi. layers for a dual-band MWIR/LWIR nBn device were sequentially grown on a Te-doped 3-inch GaSb substrate by molecular beam epitaxy (MBE) as follows: n-type InAs/GaSb 10/10 MLs “bottom contact”, unintentionally doped (u.i.d) InAs/GaSb 10/10 MLs “MWIR absorber”, u.i.d InAs/GaSb 4/9 MLs “barrier”, u.i.d InAs/GaSb 14/7 MLs “LWIR absorber”, and n-type InAs/GaSb 14/7 MLs “top contact” layers. Figure 2 shows the photoluminescence (PL) graph of the grown epi. structure at 77 K. The PL peak meaning the bandgap energy exhibits that MWIR and LWIR absorbers were grown as designed in Fig. 1.

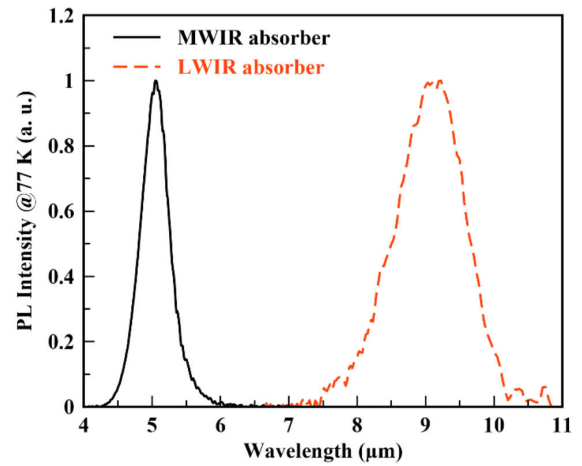


Fig. 2. PL graph of MWIR and LWIR absorbers in the grown epi. structure.

## 3. Device fabrication

In a dual-band nBn device, each pixel and common electrodes are formed on the top and bottom layers, respectively, of the grown epi. structure. Then, MWIR and LWIR bands are individually detected by a bias direction applied to the pixel electrode: negative (–) bias for MWIR and positive (+) bias for LWIR. The one-band nBn devices were fabricated through the steps of pixel isolation, post-treatment, passivation, and metallization processes [12–16]. However, the dual-band nBn device should be dry-etched more deeply than the one-band nBn device for pixel isolation because of the thicker absorber layer. And the surface of the etched absorber could be more unstable due to a longer plasma exposure time. Therefore, a two-step MESA process for the dual-band nBn device is proposed as shown in Fig. 3. First, LWIR absorber of each pixel was isolated by fully etching from the top contact layer to the barrier layer using inductively coupled plasma reactive ion etch (ICPRIE) under following conditions [15]: process temperature 200 °C, working pressure  $6.66 \times 10^{-4}$  kPa,  $\text{BCl}_3$  flow 5 sccm, RF power 270 W, and ICP power 300 W. And then, to alleviate a potential surface damage of the etched LWIR absorber caused by plasma radicals, hydrogen ( $\text{H}_2$ ) plasma treatment was *in situ* performed using ICPRIE under following conditions [16, 17]: process temperature 200°C, working pressure  $6.66 \times 10^{-4}$  kPa,  $\text{H}_2$  flow 5 sccm, RF power 30 W, and ICP power 500 W. After  $\text{SiO}_2$  passivation film was deposited using an inductively coupled plasma chemical vapour deposition (ICPCVD) equipment to protect the surface of the LWIR absorber, the first MESA process for isolating the LWIR pixels was finished.

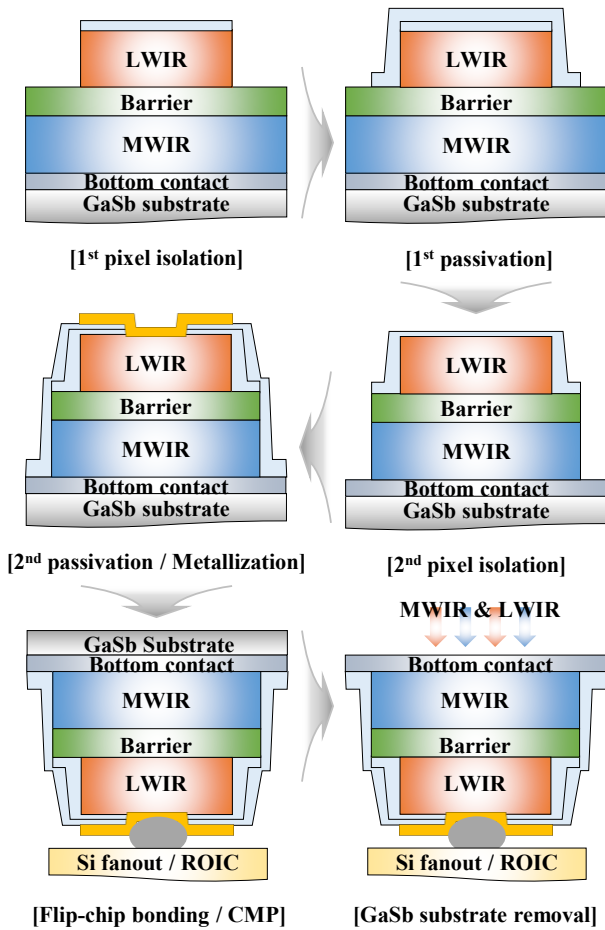


Fig. 3. Cross-sectional schematics of fabrication processes for a dual-band MWIR/LWIR device.

Second, MWIR absorber of each pixel was isolated by fully etching from the barrier layer to the bottom contact layer under the same conditions as the pixel isolation process of the LWIR absorber. Next, plasma treatment and passivation processes were also performed with the same conditions of the LWIR process. To minimize plasma exposure time of the LWIR and MWIR surfaces, it was named a 2-step MESA that each absorber was individually formed in this work. Finally, the dual-band MWIR/LWIR device was completed after the contact metals (Ti/Pt/Au) were e-beam evaporated for each pixel and common electrodes.

To evaluate electrical and optical properties of the fabricated device, the device was flip-chip bonded with Si-fanout or ROIC where indium bumps were formed. GaSb substrate of the hybridized chip had a thickness of several  $\mu\text{m}$  by a chemical-mechanical polishing (CMP) process. After that, the GaSb substrate was removed with  $\text{CrO}_3$ -based solution since it absorbs overall IR bands.

#### 4. Characteristics of dual-band MWIR/LWIR device

Figure 4 shows the dark current density of the fabricated devices. In a  $20\ \mu\text{m}$  pitch FPA, the device fabricated by a 1-step MESA process has a pixel area of  $17 \times 17\ \mu\text{m}^2$  [Fig. 4(a)], while LWIR and MWIR absorbers fabricated by a 2-step MESA process have an area of  $13 \times 13\ \mu\text{m}^2$  and  $17 \times 17\ \mu\text{m}^2$ , respectively [Fig. 4(b)]. The dark current

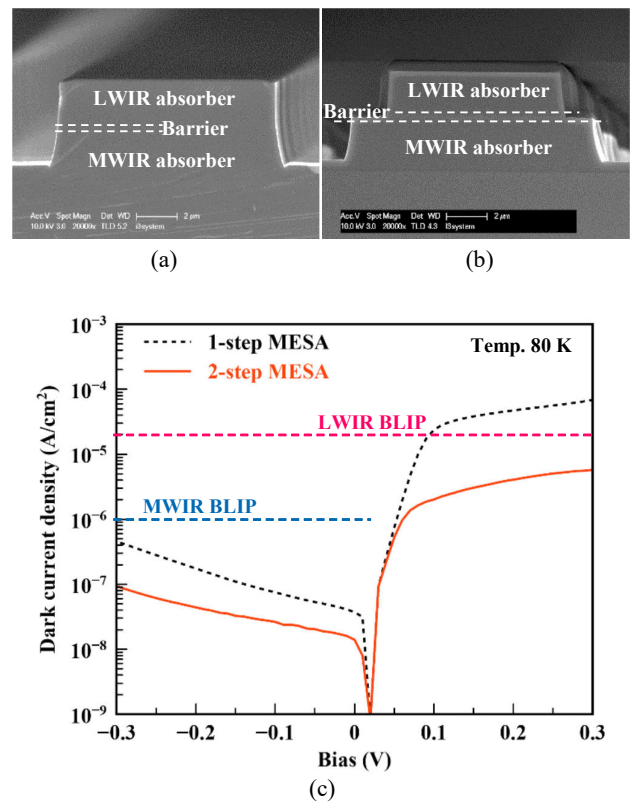


Fig. 4. Cross-sectional SEM images of the device fabricated by 1-step MESA (a) and 2-step MESA (b) processes, and comparison of the dark current density at 80 K (c).

density of the MWIR devices achieved the background limited infrared photodetection (BLIP) condition regardless of the MESA process. However, the dark current density of the LWIR device achieved the BLIP condition only when it was fabricated by the 2-step MESA process. The results mean that the proposed 2-step MESA process is suitable because it minimizes plasma damage on the LWIR surface in a dual-band device that should have the deep dry-etched pixels.

In this work, a cold filter which can transmit both MWIR and LWIR bands was developed to detect dual-band: MWIR band is  $3.7\text{--}4.8\ \mu\text{m}$  and LWIR band is  $7.7\text{--}9.4\ \mu\text{m}$ . Figure 5(a) shows the spectral QE of the dual-band device when both MWIR and LWIR absorbers have a thickness of  $2\ \mu\text{m}$ . An average QE of MWIR and LWIR devices was  $\sim 33.7\%$  and  $31.2\%$ , respectively. Generally, a spectral crosstalk [(A) in Fig. 5(a)], which is caused by absorbing MWIR band of the LWIR device, is a key issue in dual-band MWIR/LWIR detectors [9–11]. The spectral crosstalk in Fig. 5(a) was  $\sim 25.1\%$ , which is not significantly different from the average QE of the MWIR and LWIR bands. When the LWIR device is operated to acquire the LWIR image, the MWIR image could also be interfered and obtained together. Additionally, a low average QE of the MWIR device reduces the frame rate of the detector.

To enhance the average QE of the MWIR device and to reduce a spectral crosstalk, the MWIR absorber was grown to a thickness of  $4\ \mu\text{m}$ . As shown in Fig. 5(b), the average QE of the MWIR device increased to  $\sim 53.7\%$  and a spectral crosstalk (B) decreased to  $\sim 11.1\%$ . The average QE of the LWIR device slightly decreased to  $\sim 26.9\%$ , which is a

result of shifting the resonance peaks intensities and wavelengths by the typical Fabry-Perot resonance phenomenon due to the increased overall epi. thickness.

Even though the MWIR absorber was thickened, the dark current density of both MWIR and LWIR devices achieved the BLIP condition as shown in Fig. 6.

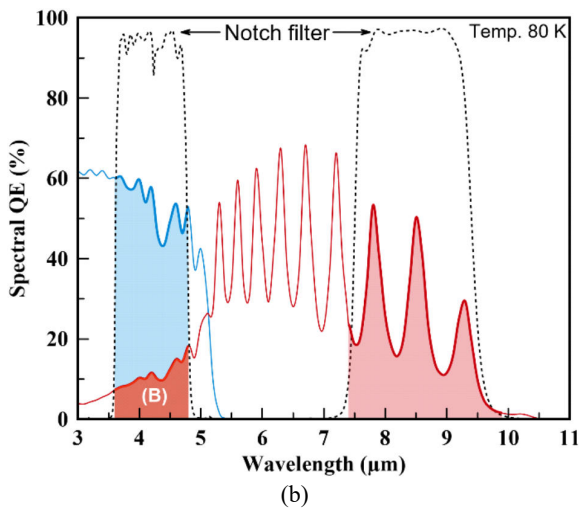
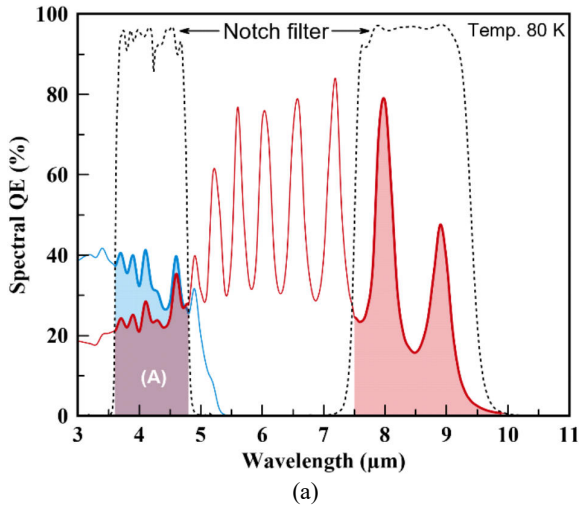


Fig. 5. Spectral QE of the fabricated dual-band MWIR/LWIR device due to the difference in thickness of the MWIR absorber: 2  $\mu\text{m}$  (a) and 4  $\mu\text{m}$  (b).

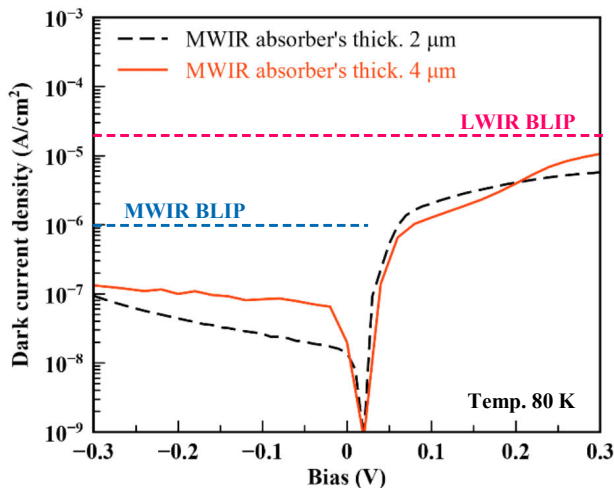


Fig. 6 Dark current comparison due to the difference in thickness of the MWIR absorber.

## 5. 20 $\mu\text{m}$ VGA dual-band MWIR/LWIR FPA

The dual-band MWIR/LWIR FPA with a MWIR absorber of 4  $\mu\text{m}$  in Figs. 5(b) and 6 was hybridized to a 20  $\mu\text{m}$  pitch 640  $\times$  512 ROIC designed by i3system, Inc. (detail specifications are listed in Table 1).

Table 1.  
Specifications of dual-band MWIR/LWIR ROIC.

Parameters	Value
Pitch	20 $\mu\text{m}$
Format	640 $\times$ 512
Integration mode	ITR <sup>a</sup>
Max. frame rate	200 Hz
Well capacity	For each MWIR/LWIR
	2.5 Me- @MWIR
	9.0 Me- @LWIR

<sup>a</sup>Integration then read.

The hybrid-chip mounted in the experimental dewar was measured at an operating temperature of 80 K. The optical properties were analysed after the image data were taken with the optics of F/2.0 and for a temperature of 293 K and 308 K of the black body. Figure 7 shows the NETD histograms, or Gaussian distribution, of the two-point corrected images for each MWIR and LWIR operation modes. Each average NETD of MWIR and LWIR modes was  $\sim 22.5$  mK and  $\sim 25.0$  mK, respectively. The operability of the hybrid-chip was  $\sim 99.9\%$  for MWIR mode and  $\sim 99.3\%$  for LWIR at  $\pm 30\%$  of an average response and two times of an average NETD.

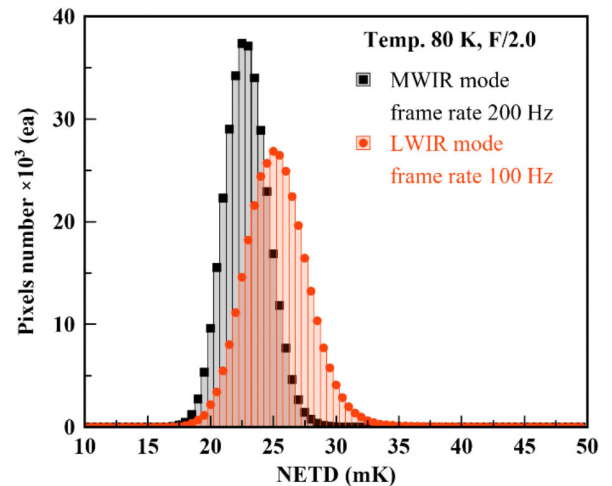


Fig. 7. NETD histogram taken with a dual-band MWIR/LWIR hybrid-chip.

## 6. Conclusions

In this work, the 20  $\mu\text{m}$  pitch 640  $\times$  512 dual-band MWIR/LWIR FPA was designed, fabricated, and evaluated. The LWIR absorber, barrier and MWIR absorber of epi. structure based on InAs/GaSb nBn were designed by the eight-band  $\mathbf{k}\cdot\mathbf{p}$  numerical method. The two-step MESA process was proposed to minimize plasma damage of the LWIR absorber. The fabricated dual-band

device with one electrode (bump) detected individually MWIR and LWIR bands by bias direction and had the dark current density achieving the BLIP condition. The device with a thick MWIR absorber increased QE of the MWIR band and reduced the spectral crosstalk. Consequently, the 20  $\mu\text{m}$  pitch  $640 \times 512$  dual-band MWIR/LWIR FPA hybridized with ROIC had the NETD of less than 30 mK and operability of more than 99% at 80 K.

### Acknowledgement

The authors gratefully acknowledge the financial support provided by Agency for Defense Development in Korea.

### References

- [1] Kim, T., Lee, H., Bae, J. & Kim, T. Susceptibility of combat aircraft modeled as an anisotropic source of infrared radiation. *IEEE Trans. Aerosp. Electron. Syst.* **52**, 2467–2476 (2016). <https://doi.org/10.1109/TAES.2016.150513>
- [2] Rogalski, A., Kopytko, M. & Martyniuk, P. *Antimonide-Based Infrared Detectors – A New Perspective*. (SPIE, 2019). <https://spie.org/Publications/Book/2278813>
- [3] Reago, D., Horn, S., Cambell, J. & Vollmerhausen, R. Third-generation imaging sensor system concepts. *Proc. SPIE* **3701**, 108 (1999). <https://doi.org/10.1117/12.352991>
- [4] Norton, P. Third-generation sensors for night vision. *Opto-Electron. Rev.* **14**, 1–10 (2006). <https://doi.org/10.2478/s11772-006-0001-5>
- [5] Rogalski, A., Antoszewski, J. & Faraone, L. Third-generation infrared photodetector arrays. *J. Appl. Phys.* **105**, 091101 (2009). <https://doi.org/10.1063/1.3099572>
- [6] Reine, M. B. HgCdTe photodiodes for IR detection: a review. *Proc. SPIE* **4288**, VI (2001). <https://doi.org/10.1117/12.429413>
- [7] Zanatta, J. et al. Single- and two-color infrared focal plane arrays made by MBE in HgCdTe. *Proc. SPIE* **4130**, 441 (2000). <https://doi.org/10.1117/12.409885>
- [8] Tennant, W. et al. A novel simultaneous unipolar multispectral integrated technology approach for HgCdTe IR detectors and focal plane arrays. *J. Electron. Mater.* **30**, 590–594 (2001). <https://doi.org/10.1007/BF02665839>
- [9] Myers, S. et al. Comparison of superlattice based dual color nBn and pBp infrared detectors. *Proc. SPIE* **8155**, 815507-1 (2011). <https://doi.org/10.1117/12.894986>
- [10] Plis, E. et al. High performance dual-band InAs/GaSb SLS detectors with nBn and pBp architectures. *Proc. SPIE* **8012**, 80120X-1 (2011). <https://doi.org/10.1117/12.882399>
- [11] Gautam, N. et al. Three color infrared detector using InAs/GaSb superlattices with unipolar barriers. *Appl. Phys. Lett.* **98**, 121106 (2011). <https://doi.org/10.1063/1.3570687>
- [12] Lee, H. et al. Comparative advantages of a type-II superlattice barrier over an AlGaSb barrier for enhanced performance of InAs/GaSb LWIR nBn photodetectors. *Opt. Lett.* **46**, 3877–3880 (2021). <https://doi.org/10.1364/OL.435479>
- [13] Jang, A. et al. Effect of Barrier Layer on InAs/GaSb Type-II Superlattice nBn Detector. in *2021 International Conference on Electronics, Information, and Communication (ICEIC)* 1–3 (2021). <https://doi.org/10.1109/ICEIC51217.2021.9369773>
- [14] Lee, H. et al. Dark current improvement due to dry-etch process in InAs/GaSb type-II superlattice LWIR photodetector with nBn structure. *Infrared Phys. Technol.* **94**, 161–164 (2018). <https://doi.org/10.1016/j.infrared.2018.09.009>
- [15] Jung, H. et al. Investigation of ICP dry etching of InAs/GaSb type-II superlattice LWIR photodetector. *Proc. SPIE* **11741**, 117411V (2021). <https://doi.org/10.1117/12.2588043>
- [16] Kang, K. et al. Dark current improvement by an in-situ plasma treatment on type-II superlattice LWIR photodetectors. *Proc. SPIE* **11741**, 117411U (2021). <https://doi.org/10.1117/12.2588041>
- [17] Lee, H. et al. Plasma treatment for surface stabilization in InAs/GaSb type-II superlattice LWIR and VLWIR photodetectors. *J. Electron. Mater.* **51**, 4689–4694 (2022). <https://doi.org/10.1007/s11664-022-09703-7>